



Full Length Article

Surface functionalization of nitrogen-doped carbon derived from protein as anode material for lithium storage

Geon-Hyoung An^a, Hyeonjin Kim^b, Hyo-Jin Ahn^{a,b,*}^a Program of Materials Science & Engineering, Convergence Institute of Biomedical Engineering and Biomaterials, Seoul National University of Science and Technology, Seoul 139-743, Republic of Korea^b Department of Materials Science and Engineering, Seoul National University of Science and Technology, Seoul 139-743, Republic of Korea

ARTICLE INFO

Keywords:

Li-ion battery
Anode
Carbon
Protein
Nitrogen-doping
Crystallizability

ABSTRACT

Carbon has received an intensive consideration in view of its application as an anode in lithium storage and is characterized by high electrical conductivity, excellent chemical and physical properties, and outstanding stability for insertion and deinsertion of Li ions. However, the due to the high-cost production requiring a high temperature process, a limited storage capacity, and a poor rate capability. In the present study, we suggest a novel protein as a raw material of carbon using simply carbonization. The nitrogen-doped carbon indicates the nitrogen (N)-doped sites with graphitic-N and pyridinic-N sites, as well as high crystallizability. The optimized electrode delivers an excellent cycling stability (284 mA h g⁻¹ after 100 cycles at 100 mA g⁻¹), an impressive rate performance (154 mA h g⁻¹ at 2000 mA g⁻¹), and a remarkable ultrafast cycling stability (112 mA h g⁻¹ after 500 cycles at 2000 mA g⁻¹). Therefore, this unique nitrogen-doped carbon offers attractive advantages in terms of the functional N-doped sites, a simple fabrication process, and a low-cost production.

1. Introduction

In the future technological life, energy is an essential demand for use in electric vehicle, electric robotics, and so on [1–3]. Therefore, a large number of approaches have been performed to respond to the ever-increasing requirements of energy storage. In this regard, due to their high energy density, high average output voltage, long cycle life, eco-compatibility, low self-discharge rate, and low memory loss, lithium ion batteries (LIBs) can be considered as a promising storage technology for portable electronic devices such as smart phones, cameras, laptops, etc. [4–7] LIBs are composed of four main components: the anode electrode, cathode electrode, separate, and electrolyte. Among them, the storage capacities and cost of anode materials of LIBs still cannot gratify the fast development of future applications such as electric vehicles and electric robotics [8–10]. Graphite anode with a limited storage capacity and a poor rate capability, which is mostly used in commercial LIBs, is commonly synthesized from oil residues such as coal-tar pitch and petroleum coke at the high temperature of 2000–3000 °C, leading to a high-cost production [11–15]. Therefore, extensive research has sought to explore functional carbon with high capacity, high-rate capability, easy approach, and low cost to replace conventional graphite.

Previous studies have focused on various carbons as anode materials for LIBs, including carbon nanofibers [16,17], carbon nanotubes [18], and graphene [19,20]. However, most of the fabrication processes require a particular precursor, unique equipment, and intricate process. Thus, as a renewable source, biomasses such as coffee shells [21], coconut [22], rice straw [23], and cherry stones [24] have recently acquired much consideration as promising candidates in the fabrication of carbon. The main reason of this interest was the abovementioned biomaterials' low cost and richness. In addition, it is widely known that the physicochemical properties of carbon-based systems can be modified by means of surface dopants [25–28]. The N-doped carbon can be further increased to active sites and defects sites, leading to an improvement of electrochemical performance [29–31]. Specifically, the defects sites onto the surface can be helped to provide electrochemical reaction sites for Li⁺ adsorption to increase the rate performance at high current densities. However, the formation of N-doping sites in carbon implies a unique synthetic method, such as the hydrothermal method, as well as an additional precursor for doping sites, which creates some challenges. Said differently, the fabrication of N-doped carbon from natural biomasses with ample amounts of nitrogen appears to be a very attractive alternative.

In addition, another issue related to the application of carbon as an

* Corresponding author at: Department of Materials Science and Engineering, Seoul National University of Science and Technology, Seoul 139-743, Republic of Korea.

E-mail address: hjahn@seoultech.ac.kr (H.-J. Ahn).

<https://doi.org/10.1016/j.apsusc.2018.08.201>

Received 2 May 2018; Received in revised form 10 August 2018; Accepted 23 August 2018

Available online 24 August 2018

0169-4332/ © 2018 Elsevier B.V. All rights reserved.

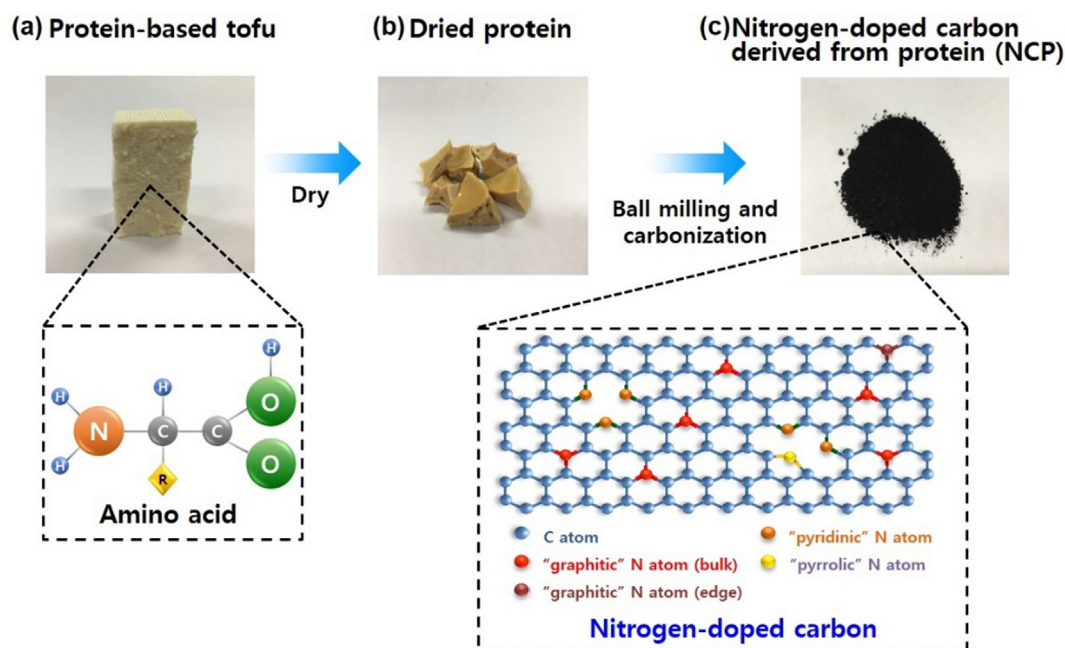


Fig. 1. Schematic illustration of the fabrication process for (a) protein-based tofu, (b) dried protein, and (c) nitrogen-doped carbon derived from protein (NCP).

anode material is ultrafast performance to extend the LIB applications [3,5,16]. The ultrafast performance of N-doped carbon is more favorable than that conventional graphite due to the excellent Li⁺ adsorption of the latter that results from defects sites [11].

Therefore, in the present study, we prepared N-doped carbon derived from protein as anode material for LIBs. The protein, which contains amino acid with carbon, nitrogen, oxygen, and hydrogen, is one of the novel carbon sources [32,33]. The N-doped carbon area was developed using carbon and nitrogen atoms. Moreover, we demonstrated and optimized the electrochemical performance of N-doped carbon from protein by definite conditions using the optimized synthetic temperature. Our concept would widen the synthesis of carbon from biomass and could contribute to the development of anode materials for high-performance LIBs, including ultrafast performance.

2. Experimental

2.1. Synthesis of nitrogen-doped carbon derived from protein (NCP)

Protein from tofu (Pulmuone Co., Ltd.) was used. The nitrogen-doped carbon derived from protein (NCP) was simply synthesized by carbonization. The protein was firstly dried in an oven at 100 °C to take out water, and then heated at 400 °C for 3 h with the heating rate of 10 °C min⁻¹ to remove any impurities as organic materials. Afterwards, to eliminate the inorganic materials, the prepared sample was washed using nitric acid. Finally, the carbonization was performed in N₂ atmosphere. To obtain the optimization of energy storage performance in LIBs, the carbonization was gradually performed using different temperatures of 1100, 1200, and 1300 °C for 2 h with the heating rate of 10 °C min⁻¹, which are henceforth referred to as NCP 1100, NCP 1200, and NCP 1300, respectively.

2.2. Characterization

The structure and morphology were inspected using scanning electron microscopy (SEM, Hitachi S-4800), and transmission electron

microscopy with dispersive spectrometer (TEM-EDS, KBSI Gwangju Center, Tecnai G²). To investigate the crystal structure, X-ray diffractometry (XRD, Rigaku, D/Max 2500 V) was confirmed in the range from 10° to 90° and by a Cu K_α source. The empirical parameter of intensities for main peaks was used to investigate the crystallinity of carbon. Thus, the ratio of height of the main peak to the background was calculated. Also, the standard deviation of the calculated data is ± 0.1. X-ray photoelectron spectroscopy (XPS, Thermo scientific, ESCALAB 250) was used to analyze the chemical bonding states. The binding energies of the XPS peaks were calibrated by the C 1s core level (284.5 eV) before fitting.

2.3. Electrochemical characterization

Energy storage performance with electrochemical reactions were executed by the half-cell system using coin cells (CR2032). The working electrode was fabricated on copper foil substrate as the current collector from a slurry, made up of the NCP as the active material (80 wt%), Ketjen black (10 wt%) as the conducting material, and polyvinylidene difluoride (10 wt%) as the binder. The prepared electrode was dried in an oven at 100 °C for 10 h. The Li metal foil and a porous polypropylene membrane were used for the counter electrode and the separator, respectively, in a 1.0 M LiPF₆ solution in a mixture of ethylene carbonate dimethyl carbonate (1:1) as the electrolyte. The coin cells were prepared in a argon-filled glove box with O₂ and H₂O contents less than 5 ppm. The charging/discharging measurements were tested in the potential range of 0.05–3.00 V (vs Li/Li⁺) at the current density of 100 mA g⁻¹ up to 100 cycles at 25 °C. The rate capability test was observed at the following current densities: 100, 300, 500, 700, 1000, and 2000 mA g⁻¹. The ultrafast cycling stability was examined at the current density of 2000 mA g⁻¹ up to 500 cycles.

3. Results and discussion

Fig. 1 elucidates the synthesis process of NCP by the protein using a facile method, including the dry procedure and carbonization. The

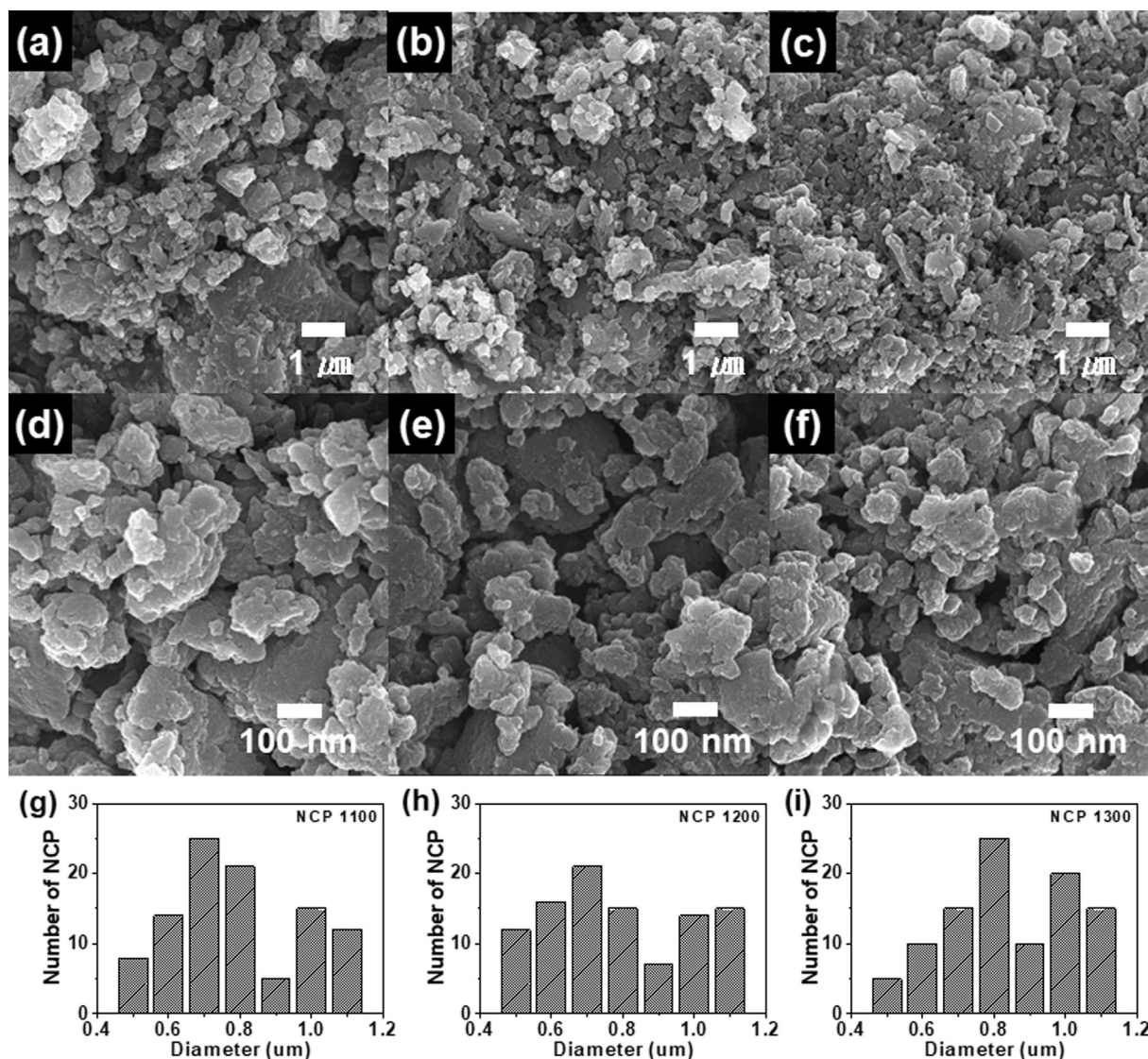


Fig. 2. (a–c) Low-magnification and (d–f) high-magnification SEM images of NCP 1100, NCP 1200, and NCP 1300. The particle size distribution of (g) NCP 1100, (e) NCP 1200, and (f) NCP 1300.

protein (see Fig. 1a) consisting of an amino acid was prepared as the raw material for carbon due to its carbon and nitrogen source. The protein was dried to remove the water, as shown in Fig. 1b. Afterwards, the as-prepared sample was pulverized and then carbonized under the nitrogen atmosphere. As a result, NCP (see Fig. 1c) was successfully synthesized with various carbonization temperature to obtain the optimum condition in electrochemical performance.

Fig. 2a–f shows the SEM images of NCP 1100 (Fig. 2a and d), NCP 1200 (Fig. 2b and e) and NCP 1300 (Fig. 2c and f), respectively. The morphology of NCP indicates a block-like shape. The main distribution of particle sizes for NCP 1100 (Fig. 2g), NCP 1200 (Fig. 2h), and NCP 1300 (Fig. 2i) gradually moved to large size section due to a high carbonization temperature. To further survey the nanostructural features of NCP, the TEM measurements were performed.

Fig. 3a–f shows the TEM images of NCP 1100 (Fig. 3a and d), NCP 1200 (Fig. 3b and e), and NCP 1300 (Fig. 3c and f), respectively. All samples showed a uniform contrast, involving only a single phase of carbon. In addition, as the temperature of carbonization increased, NCP

1200 (Fig. 3e) and NCP 1300 (Fig. 3f) exhibited the localized nanocrystallites structure at the edge, which is favourable for the adsorption and intercalation of Li ions [34–36]. Moreover, the crystalline nanostructures of NCP 1100, NCP 1200, and NCP 1300 were proved by the selected area electron diffraction patterns (see Fig. 3d–f, inserted images). With an increase of the temperature, the dispersed diffraction rings gradually faded up, implying an improvement of the graphitic local structure. Fig. 3g presents TEM–EDS mapping data of NCP 1200, implying the evenly homogeneous distribution of carbon and nitrogen.

The XRD patterns of NCP 1100, NCP 1200, and NCP 1300 are shown in Fig. 4a–c, respectively. All XRD patterns are observed using two broad peaks at around 24° and 43° , which can be attributed to the (0 0 2) and (1 0 0) planes of amorphous carbon, respectively. Furthermore, from the (0 0 2) peak of graphitic layers, the empirical parameter was calculated to investigate the crystallizability by the ratio of height of the (0 0 2) peak to the background [37–39]. The empirical parameter of NCP 1300 had the high value of 16.7 as compared to NCP 1100 (16.1) and NCP 1200 (16.5), suggesting that an increase of the

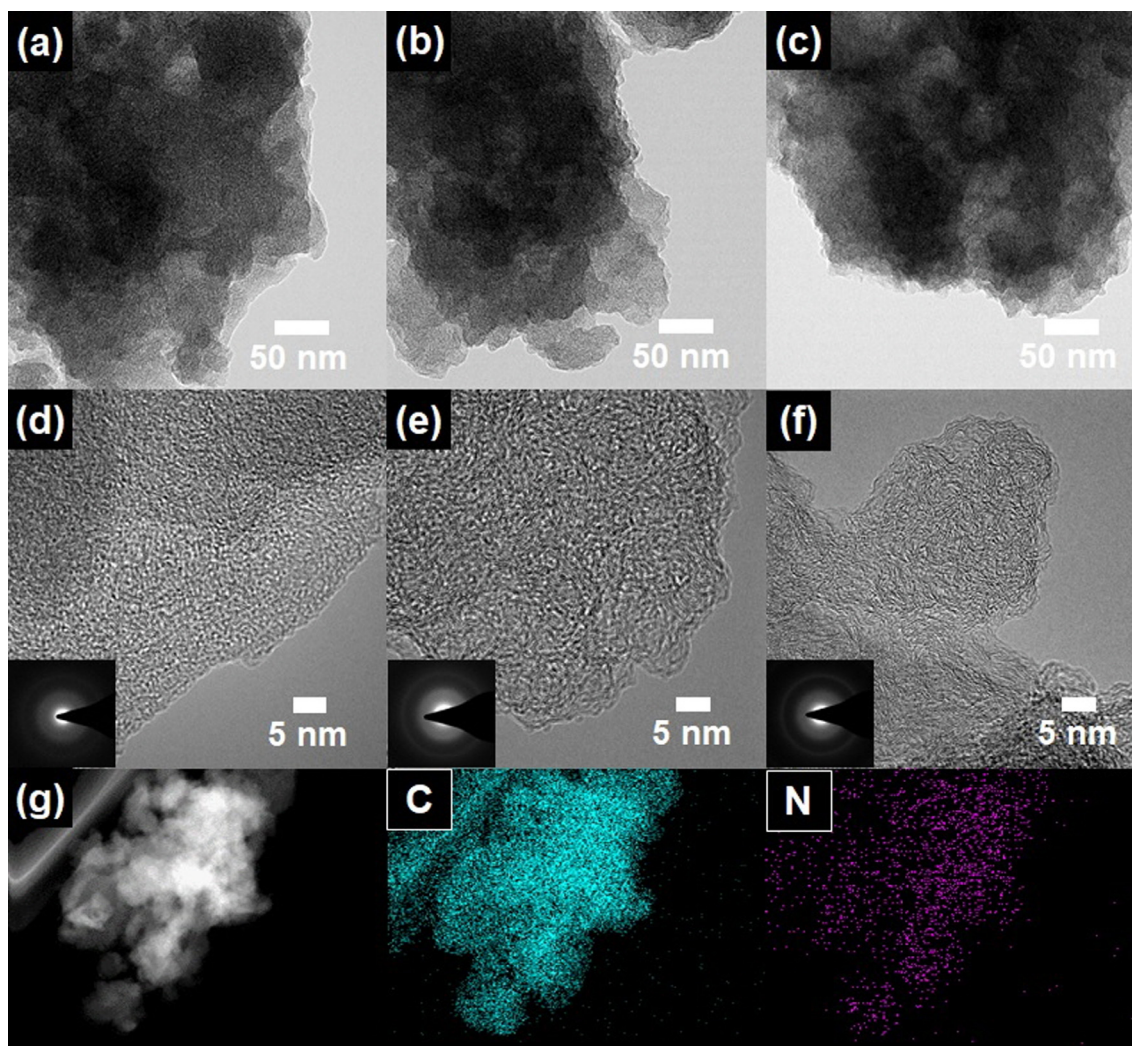


Fig. 3. (a–c) Low-magnification and (d–f) high-magnification TEM images of NCP 1100, NCP 1200, and NCP 1300. (g) TEM-EDS spectra of NCP 1200.

temperature may result in a higher degree of graphitization of the structure. Thus, the XRD results mean that the different crystallinity of NCP 1100, NCP 1200, and NCP 1300 is attributed to the increased carbonization temperature. The high crystallizability of carbon could provide the excellent cycling stability in LIBs.

The surface elemental compositions of NCP 1100, NCP 1200, and NCP 1300 were examined by the XPS measurement. Fig. 5a–c presents the full scan spectrum of NCP 1100, NCP 1200, and NCP 1300, respectively, consisting of O 1s, N 1s and C 1s spectra, implying the existence of O, N, and C, element compositions without other impurity phases. The C 1s spectrums of NCP 1100, NCP 1200, and NCP 1300 were C–C groups (284.5 eV), C–N groups (285.5 eV), C–O groups (286.5 eV), and N=C–O groups (288.1 eV), respectively [40–42] (see Fig. 5d–f). With an increase of the carbonization temperature from 1100 to 1300 °C, the concentration of N atom decreased to 6.3, 5.2, and 4.7 at%, respectively (see Fig. 5g–i). The carbonization temperature has a significant effect on the N atom content into the carbon, indicating that the concentration of N atom was reduced in a high carbonization temperature due to the increased atom ratio of C, as well as due to a higher degree of graphitization of the structure. In general, N 1s spectra of N-doped carbon can be divided to four nitrogen species such as pyridinic-N, pyrrolic-N, graphitic-N, and pyridine-N-oxide, which can

be further increased to electrochemical active sites, leading to an enhancement of electrochemical performance [43–47]. Thus, for all samples, the N 1s spectra can be divided using the XPS peak fitting program (XPSPEAK Version 4.1) into four peaks located at 398.3, 400.2, 401.1, and 403.1 eV, which are identified to pyridinic-N, pyrrolic-N, graphitic-N, and pyridine-N-oxide, respectively [46,47]. Particularly, they showed a higher concentration of graphitic-N and pyridinic-N, respectively. The concentrations of pyridinic-N, pyrrolic-N, graphitic-N, and pyridine-N-oxide are summarized in Table 1. The graphitic-N peak can provide an improved electrical conductivity resulting from the graphitic N embeds into the honeycomb carbon, leading to rate capability in LIBs [43–45]. Furthermore, the pyridinic-N can constitute many active sites and extrinsic defects and provide a high electrochemical performance with a low energy barrier for the insertion of Li ion, leading to an improvement of reversible capacity in LIBs [43–45]. Compared to the traditionally post-modification process using the additional nitrogen source, our approach offers a unique and economic method to obtain the N-doped carbon.

As shown in Fig. 6a–c, NCP 1100, NCP 1200, and NCP 1300 electrodes demonstrate typical voltage capacity profiles of carbon anodes, indicating that the successful synthesis of carbon derived from protein [3,5,25]. During the discharging process, the sloping region had the

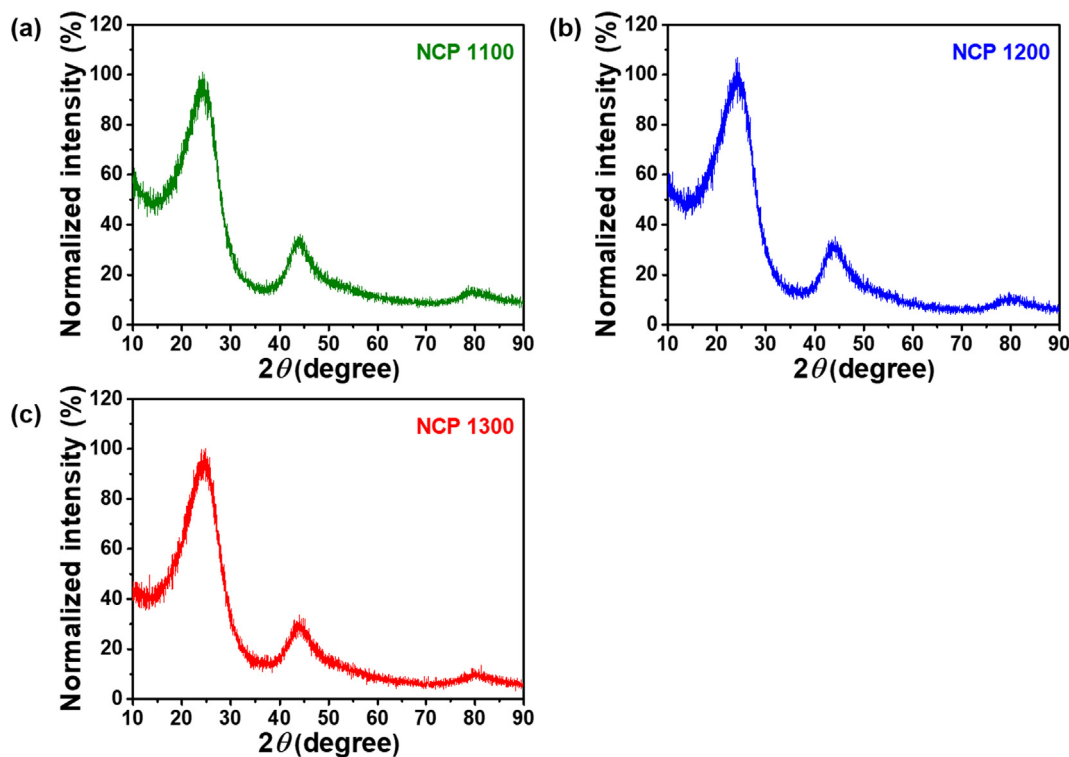


Fig. 4. The XRD patterns of (a) NCP 1100, (b) NCP 1200, and (c) NCP 1300.

voltage plateau under 1.00 V, meaning that more Li ions partake in the electrochemical reaction at a low potential. Also, the charging curve rise in a voltage ranges from 0.05 to 3.00 V. In addition, due to the development of a solid electrolyte interphase (SEI) film from electrolyte decomposition on the electrode surface, the large initial irreversible capacity of all electrodes appeared [6,9,20].

Coulombic efficiency of NCP 1100, NCP 1200, and NCP 1300 electrodes over 100 cycles at the current density of 100 mA g^{-1} are shown in Fig. 7a. Due to the development of SEI layer on the electrode surface, all electrodes indicated the low initial Coulombic efficiency at the first cycle. Notwithstanding, NCP 1100 electrode revealed a highest initial Coulombic efficiency of 57% as compared to NCP 1200 electrode (55%) and NCP 1300 electrode (49%), indicating that the N-doped sites of carbon could improve the initial Coulombic efficiency. In addition, the reversible capacity of all electrodes reached 100%, meaning the excellent reversible activity. Fig. 7b displays the cycling stability with the discharge capacities of NCP 1100, NCP 1200, and NCP 1300 electrodes over 100 cycles at the current density of 100 mA g^{-1} . NCP 1100 electrode exhibited high discharge capacities of 394 mA h g^{-1} after 2 cycles, as compared to the NCP 1200 electrode (349 mA h g^{-1}) and NCP 1300 electrode (303 mA h g^{-1}). These results confirm that the improved energy storage performance of NCP 1100 electrode is attributed to the large number of N-doped sites with a low energy barrier for the Li ion insertion. By contrast, the cycling stability of NCP 1100 electrode after 100 cycles has the lowest value of 75% due to its low crystallizability. On the other hand, NCP 1200 and NCP 1300 electrodes showed the high cycling stability of 81% and 82%, respectively, owing to high crystallizability as compared to NCP 1100 electrode. As a result, NCP 1200 presented the highest discharge capacities of 284 mA h g^{-1} after 100 cycles as compared to the NCP 1100 electrode (273 mA h g^{-1}) and NCP 1300 electrode (251 mA h g^{-1}). Therefore, the number of N-doped sites and crystallizability of NCP 1200 electrode was optimized for anode materials in LIBs. Particularly, the NCP 1200 electrode held a

higher discharge specific capacity than the previously reported electrodes using biomass such as pomelo pericarp (116 mA h g^{-1}) [48], walnut shells (200 mA h g^{-1}) [49], and microalgal biomass (160 mA h g^{-1}) [50]. Fig. 7c shows the results of the rate capability test from 100 mA g^{-1} to 2000 mA g^{-1} . Among the electrodes, NCP 1200 electrode delivered the high discharge capacities of 299, 251, 207, 190, and 154 mA h g^{-1} at the current density of 100, 300, 700, 1000, 1500 and 2000 mA g^{-1} for 10 cycles at each step, respectively. Of note, the discharge capacity could completely restore to the original value of 299 mA h g^{-1} when the current density recovered to 100 mA g^{-1} . The excellent rate capability can be ascribed to the number of N-doped sites related to the enhanced electrical conductivity resulting from the graphitic N embeds into the honeycomb carbon. The rapid growth of the LIB industry guides the high requirements as ultrafast cycling stability [51]. Fig. 7d shows the ultrafast cycling stability of NCP 1100, NCP 1200, and NCP 1300 electrodes over 500 cycles at the high current density of 2000 mA g^{-1} . As compared to NCP 1100 electrode (80 mA h g^{-1}) and NCP 1300 electrode (83 mA h g^{-1}), NCP 1200 electrode showed an impressive capability for ultrafast cycling stability with 112 mA h g^{-1} after 500 cycles. The enhanced ultrafast cycling stability of NCP 1200 electrode should be credited to the specific optimization of N-doped sites and crystallizability.

Therefore, in the present study, we demonstrated that the improved energy storage performance using the carbon derived from protein can be explained as shown in Fig. 8. The N-doped sites could efficiently deliver high discharge capacities after 2 cycles (see Fig. 8a) from numerous active sites and extrinsic defects during the insertion and deinsertion of Li ions. The crystallizability of carbon could contribute the cycling stability over 100 cycles (see Fig. 8b) due to their excellent physical property. In addition, the specific optimization of N-doped sites and crystallizability of carbon leads to the improved ultrafast cycling stability over 500 cycles at the high current density (see Fig. 8c). These results indicate that the improved performance of ultrafast

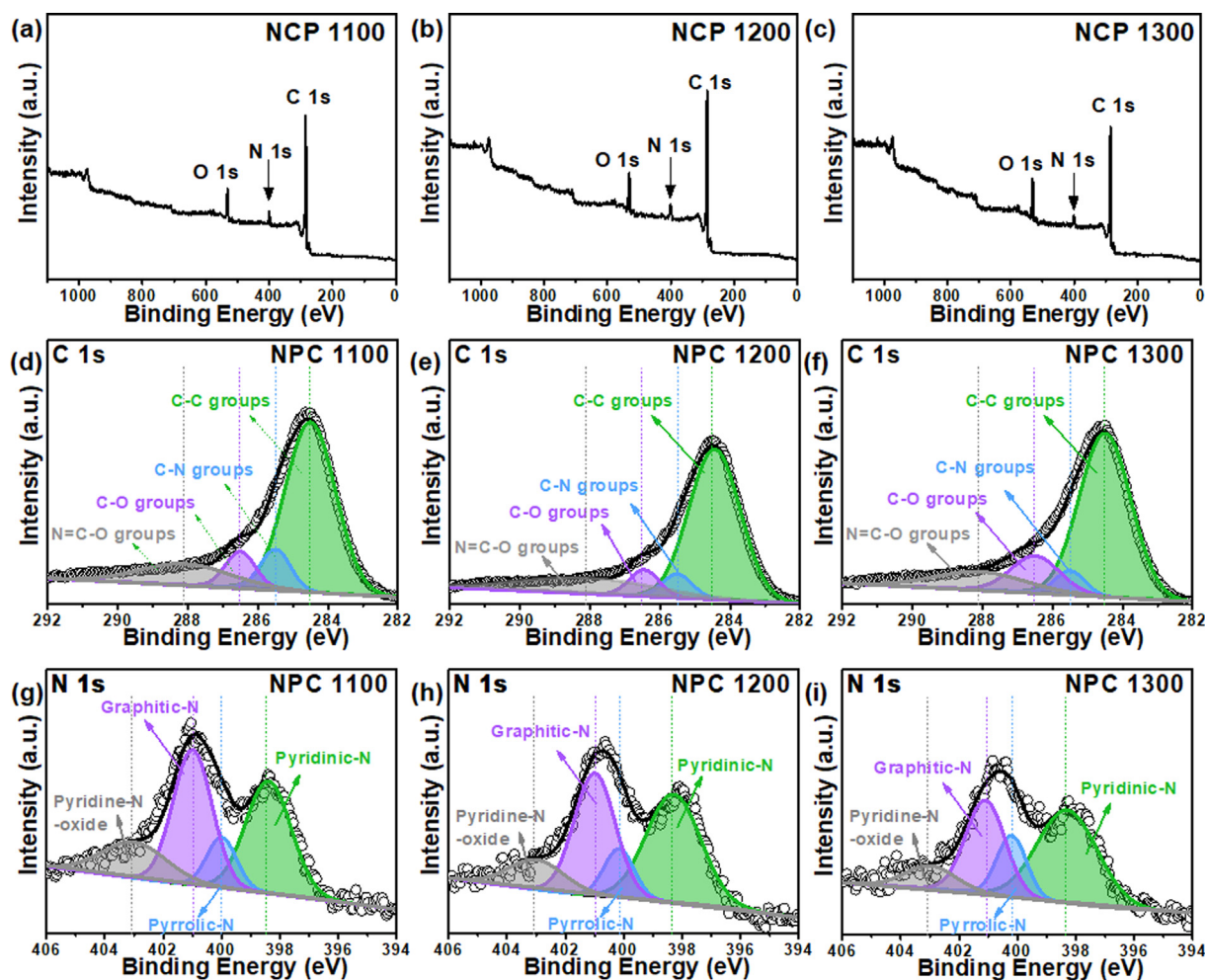


Fig. 5. The XPS spectra of (a–c) full scan spectrum, (d–f) C 1s, and (d–f) N 1s of NCP 1100, NCP 1200, and NCP 1300.

Table 1

Concentration of different nitrogen species of NCP 1100, NCP 1200, and NCP 1300.

Samples	Concentration of different nitrogen species (%)			
	Pyridinic-N (398.3 eV ± 0.1 eV)	Pyrrolic-N (400.2 eV ± 0.1 eV)	Graphitic-N (401.1 eV ± 0.1 eV)	Pyridine-N-oxide (403.1 eV ± 0.1 eV)
NCP 1100	35.8	10.5	37.2	16.5
NCP 1200	34.0	16.3	34.0	15.7
NCP 1300	33.4	18.1	33.6	14.9

cycling of NCP 1200 electrode is ascribed to the two effects. Firstly, the high amount of the N-doped sites could permit the high discharge capacity. In addition, the high crystallizability with high value of 16.5 about the ratio of height of the (0 0 2) peak to the background could enable the enhanced cycling stability.

4. Conclusions

In the present study, the protein-based NCP 1200 electrode as an

electrode material in LIBs was simply synthesized using carbonization. Of note, we suggested that the protein is a novel raw material for carbon. The optimized NCP 1200 had the N-doped sites (5.2 at%) with graphitic-N and pyridinic-N sites, as well as high crystallizability. The impressive electrochemical performances of NCP 1200 electrode with a high discharge capacity (284 mA h g⁻¹ after 100 cycles at 100 mA g⁻¹), an outstanding rate performance (154 mA h g⁻¹ at 2000 mA g⁻¹), and an excellent ultrafast cycling stability (112 mA h g⁻¹ after 500 cycles at 2000 mA g⁻¹) can definitely be ascribed to the following two effects: (i)

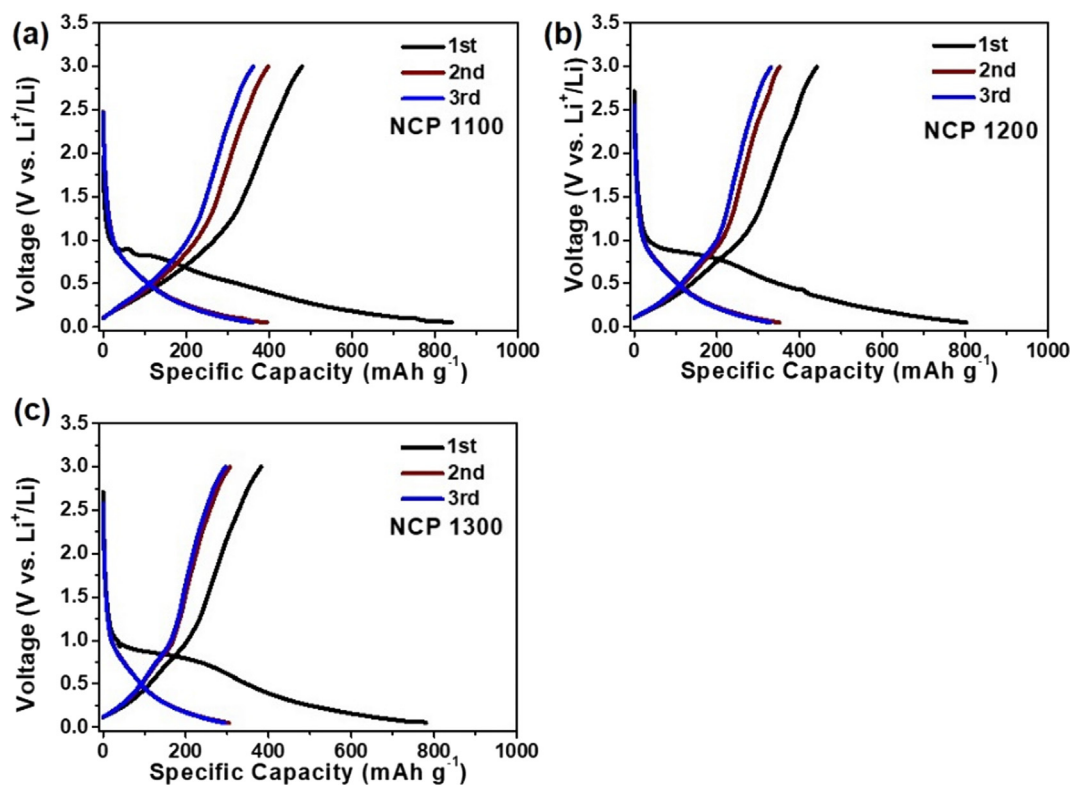


Fig. 6. Charge-discharge curves of NCP 1100, NCP 1200, and NCP 1300 electrodes at the current density of 100 mA g^{-1} in the potential range of 0.05–3.00 V for 1st, 2nd, and 3rd cycles.

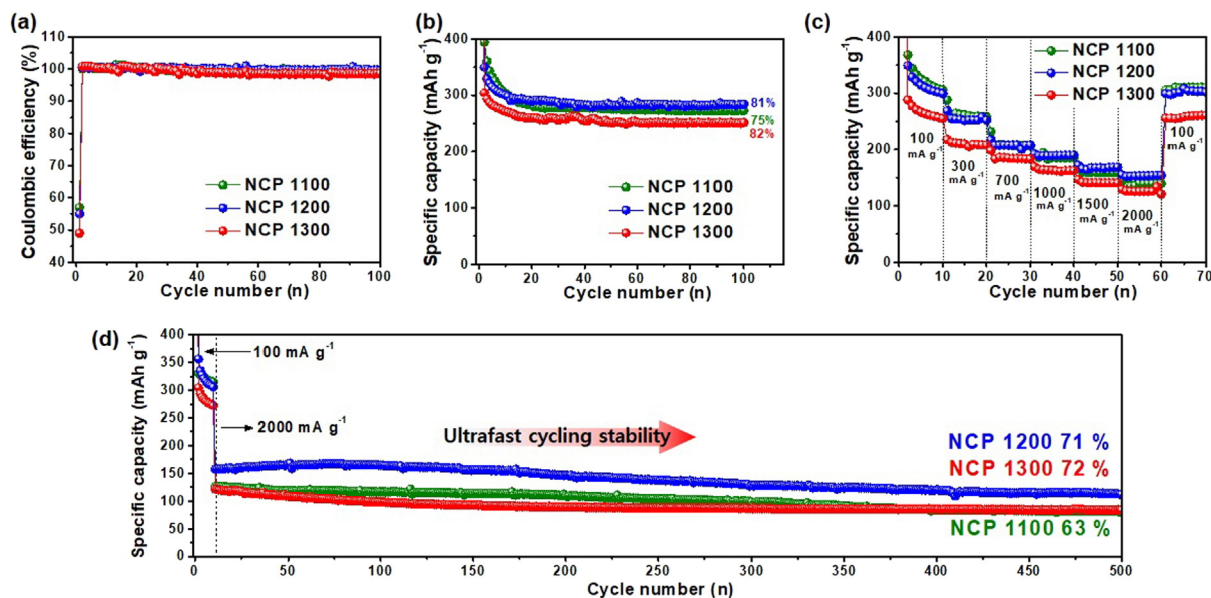


Fig. 7. (a) Coulombic efficiency, (b) cycling stability over 100 cycles at current densities of 100 mA g^{-1} . (c) rate capability at current densities of 100, 300, 500, 700, 1000, and 2000 mA g^{-1} . (d) ultrafast cycling stability over 500 cycles at the current density of 2000 mA g^{-1} .

the high discharge capacity and outstanding rate performance are due to the N-doped sites in carbon with favorable active sites and the increased electrical conductivity; (ii) the excellent cycling stability at low and high current densities is obtained using the optimization of N-

doped sites and crystallizability of carbon. Taken together, our results indicate that the protein might be one of the most powerful and promising raw materials for carbon as an anode material in LIBs.

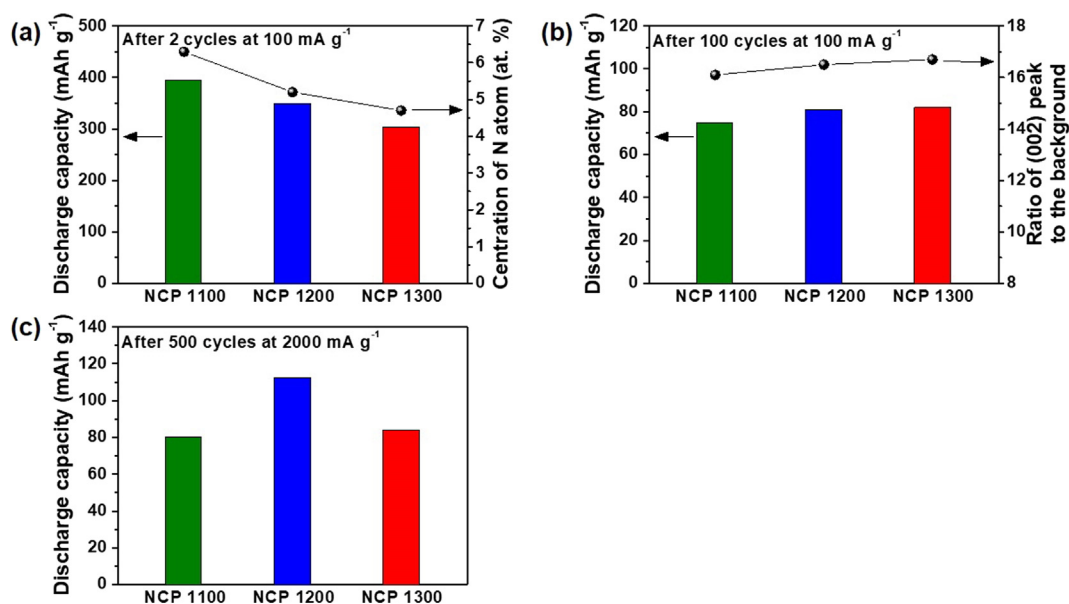


Fig. 8. (a) Relationship between the discharge capacity and the concentration of nitrogen atoms. (b) Relationship between the discharge capacity and the crystallizability. (c) The detailed value of specific capacities for ultrafast cycling stability over 500 cycles at the current density of 2000 mA g⁻¹.

Acknowledgments

This study was supported by the Advanced Research Project funded by the SeoulTech (Seoul National University of Science and Technology)

References

- P.G. Bruce, B. Scrosati, J.-M. Tarascon, Nanomaterials for rechargeable lithium batteries, *Angew. Chem. Int. Ed.* 47 (2008) 2930–2946.
- M. Armand, J.-M. Tarascon, Building better batteries, *Nature* 451 (2008) 652–657.
- G.-H. An, D.-Y. Lee, H.-J. Ahn, Tunneled mesoporous carbon nanofibers with embedded ZnO nanoparticles for ultrafast lithium storage, *ACS Appl. Mater. Interf.* 9 (2017) 12478–12485.
- M. Fang, Z. Wang, X. Chen, S. Guan, Sponge-like reduced graphene oxide/silicon/carbon nanotube composites for lithium ion batteries, *Appl. Surf. Sci.* 436 (2018) 345–353.
- G.-H. An, D.-Y. Lee, Y.-J. Lee, H.-J. Ahn, Ultrafast lithium storage using antimony-doped tin oxide nanoparticles sandwiched between carbon nanofibers and a carbon skin, *ACS Appl. Mater. Interf.* 8 (2016) 30264–30270.
- S. Guo, Y. Chen, L. Shi, Y. Dong, J. Ma, X. Chen, H. Song, Nitrogen-doped biomass-based ultra-thin carbon nanosheets with interconnected framework for high-performance lithium-ion batteries, *Appl. Surf. Sci.* 437 (2018) 136–143.
- C. Deng, Y. Liu, Z. Lu, C. Ma, T. Ge, W. Li, G. Yang, The effect of passivation film in preparation 3D structural carbon paper/tin oxide@carbon as freestanding anode for lithium-ion batteries, *Appl. Surf. Sci.* 435 (2018) 1307–1313.
- G.-H. An, D.-Y. Lee, H.-J. Ahn, Carbon-encapsulated hollow porous vanadium-oxide nanofibers for improved lithium storage properties, *ACS Appl. Mater. Interf.* 8 (2016) 19466–19474.
- Y.-W. Lee, G.-H. An, B.-S. Kim, J. Hong, S. Pak, E.-H. Lee, Y. Cho, J. Lee, P. Giraud, S.N. Cha, H.-J. Ahn, J.I. Sohn, J.M. Kim, Synergistic effects of a multifunctional graphene based interlayer on electrochemical behavior and structural stability, *ACS Appl. Mater. Interf.* 8 (2016) 17651–17658.
- Q. Wu, J. Liu, C. Yuan, Q. Li, H. Wang, Nitrogen-doped 3D flower-like carbon materials derived from polyimide as high-performance anode materials for lithium-ion batteries, *Appl. Surf. Sci.* 425 (2017) 1082–1088.
- H. Li, Z. Wang, L. Chen, X. Huang, Research on advanced materials for Li-ion batteries, *Adv. Mater.* 21 (2009) 4593–4607.
- J.H. Lee, C.S. Yoon, J.-Y. Hwang, S.-J. Kim, F. Maglia, P. Lamp, S.-T. Myung, Y.-K. Sun, High-energy-density lithium-ion battery using a carbon-nanotube-Si composite anode and a compositionally graded Li[Ni_{0.85}Co_{0.05}Mn_{0.10}]O₂ cathode, *Energy Environ. Sci.* 9 (2016) 2152–2158.
- J. Wang, P. Nie, B. Ding, S. Dong, X. Hao, H. Dou, X. Zhang, Biomass derived carbon for energy storage devices, *J. Mater. Chem. A* 5 (2017) 2411–2428.
- M.-M. Titirici, R.J. White, C. Falco, M. Sevilla, Black perspectives for a green future: hydrothermal carbons for environment protection and energy storage, *Energy Environ. Sci.* 5 (2012) 6796–6822.
- J. Deng, M. Li, Y. Wang, Biomass-derived carbon: synthesis and applications in energy storage and conversion, *Green Chem.* 18 (2016) 4824–4854.
- G.-H. An, H.-J. Ahn, Ultrafast lithium storage of high dispersed silicon and titanium oxide nanoparticles in carbon, *J. Alloy. Compd.* 710 (2017) 274–280.
- G.-H. An, H.-J. Ahn, Carbon nanofiber/cobalt oxide nanopyrmaid core-shell nanowires for high-performance lithium-ion batteries, *J. Power Sources* 272 (2014) 828–836.
- H. Liu, Y. Zou, L. Huang, H. Yin, C. Xi, X. Chen, H. Shentu, C. Li, J. Zhang, C. Lv, M. Fan, Enhanced electrochemical performance of sandwich-structured polyaniline-wrapped silicon oxide/carbon nanotubes for lithium-ion batteries, *Appl. Surf. Sci.* 442 (2018) 204–212.
- M.E. Feng, S. Wang, Y. Yu, Q. Feng, J. Yang, B. Zhang, Carboxyl functionalized carbon fibers with preserved tensile strength and electrochemical performance used as anodes of structural lithium-ion batteries, *Appl. Surf. Sci.* 392 (2017) 27–35.
- J. Han, J. Qin, L. Guo, K. Qin, N. Zhao, C. Shi, E. Liu, F. He, L. Ma, C. He, Ultrasmall Fe₂GeO₄ nanodots anchored on interconnected carbon nanosheets as high-performance anode materials for lithium and sodium ion batteries, *Appl. Surf. Sci.* 427 (2018) 670–679.
- Y.J. Hwang, S.K. Jeong, K.S. Nahm, J.S. Shin, A.M. Stephan, Pyrolytic carbon derived from coffee shells as anode materials for lithium batteries, *J. Phys. Chem. Solids* 68 (2007) 182–188.
- Y.J. Hwang, S.K. Jeong, J.S. Shin, K.S. Nahm, A.M. Stephan, High capacity disordered carbons obtained from coconut shells as anode materials for lithium batteries, *J. Alloy. Compd.* 448 (2008) 141–147.
- D.-J. Ryu, R.-G. Oh, Y.-D. Seo, S.-Y. Oh, K.-S. Ryu, Recovery and electrochemical performance in lithium secondary batteries of biochar derived from rice straw, *Environ. Sci. Pollut. Res.* 22 (2015) 10405–10412.
- J.C. Arrebola, A. Caballero, L. Hernán, J. Morales, M. Olivares-Marín, V. Gómez-Serrano, Improving the performance of biomass-derived carbons in Li-ion batteries by controlling the lithium insertion process, *J. Electrochem. Soc.* 157 (2010) A791–A797.
- A. Politano, G. Chiarello, Ice formation on clean and alkali-doped quasi-free-standing graphene: a vibrational investigation, *Carbon* 93 (2015) 242–249.
- A. Politano, V. Formoso, G. Chiarello, Chemical reactions at clean and alkali-doped mismatched metal/metal interfaces, *J. Phys. Chem. C* 113 (2009) 316–320.
- A. Politano, G. Chiarello, C.-N. Kuo, C.S. Lue, R. Edla, P. Torelli, V. Pellegrini, D.W. Boukhvalov, *Adv. Funct. Mater.* 28 (2018) 1706504.
- A. Politano, M.S. Vitiello, L. Viti, D.W. Boukhvalov, G. Chiarello, *FlatChem* 1 (2017) 60–64.
- L.L. Zhang, X. Zhao, H. Ji, M. Stoller, L. Lai, S. Murali, S. McDonnell, B. Cleveger, R.M. Wallace, R.S. Ruoff, Nitrogen doping of graphene and its effect on quantum capacitance, and a new insight on the enhanced capacitance of N-doped carbon, *Energy Environ. Sci.* 5 (2012) 9618–9625.
- V.B. Paramabhath, R. Nagar, S. Ramaprabhu, Effect of nitrogen doping on hydrogen storage capacity of palladium decorated graphene, *Langmuir* 28 (2012) 7826–7833.
- L.V. alentini, E. Braca, J.M. Kenny, G. Fedosenko, J. Engemann, L. Lozzi, S. Santucci, Nitrogen doping of fluorinated amorphous carbon thin films: structural and optical properties evolution upon thermal annealing, *Thin Solid Films* 408 (2002) 291–296.
- G.-H. An, D.-Y. Lee, H.-J. Ahn, Tofu-derived carbon framework with embedded ultrasmall tin nanocrystals for high-performance energy storage devices, *J. Alloy. Compd.* 722 (2017) 60–68.
- D.-Y. Lee, G.-H. An, H.-J. Ahn, High-surface-area tofu based activated porous carbon for electrical double-layer capacitors, *J. Ind. Eng. Chem.* 52 (2017) 121–127.
- Y. Zhu, M. Chen, Q. Li, C. Yuan, C. Wang, A porous biomass-derived anode for high-performance sodium-ion batteries, *Carbon* 129 (2018) 695–701.

- [35] M. Imtiaz, C. Zhu, Y. Li, M. Pak, I. Zada, S.W. Bokhari, Z. Chen, D. Zhang, S. Zhu, Functionalized bioinspired porous carbon with graphene sheets as anode materials for lithium-ion batteries, *J. Alloy. Compd.* 724 (2017) 296–305.
- [36] W. Yu, H. Wang, S. Liu, N. Mao, X. Liu, J. Shi, W. Liu, Shougang Chen, Xin Wang, N. O-codoped hierarchical porous carbons derived from algae for high-capacity supercapacitors and battery anodes, *J. Mater. Chem. A* 4 (2016) 5973.
- [37] J. Ou, Y. Zhang, L. Chen, Q. Zhao, Y. Meng, Y. Guo, D. Xiao, Nitrogen-rich porous carbon derived from biomass as a high performance anode material for lithium ion batteries, *J. Mater. Chem. A* 3 (2015) 6534–6541.
- [38] G.-H. An, H.-J. Ahn, Activated porous carbon nanofibers using Sn segregation for high-performance electrochemical capacitors, *Carbon* 65 (2013) 87–96.
- [39] G.-H. An, B.-R. Koo, H.-J. Ahn, Activated mesoporous carbon nanofibers fabricated using water etching-assisted templating for high-performance electrochemical capacitors, *PCCP* 18 (2016) 6587–6594.
- [40] L. Chen, Z. Hu, L. Liu, Y. Huang, A facile method to prepare multifunctional PBO fibers: simultaneously enhanced interfacial properties and UV resistance, *RSC Adv.* 3 (2013) 24664–24670.
- [41] X. Wen, J. Wu, D. Gao, C. Lin, Interfacial engineering with amino-functionalized graphene for efficient perovskite solar cells, *J. Mater. Chem. A* 4 (2016) 13482–13487.
- [42] W. Huang, S. Ptasinska, Functionalization of graphene by atmospheric pressure plasmajet in air or H₂O₂ environments, *Appl. Surf. Sci.* 367 (2016) 160–166.
- [43] H. Tao, L. Xiong, S. Du, Y. Zhang, X. Yang, L. Zhang, Interwoven N and P dual-doped hollow carbon fibers/graphitic carbon nitride: an ultrahigh capacity and rate anode for Li and Na ion batteries, *Carbon* 122 (2017) 54–63.
- [44] L. Huang, Q. Guan, J. Cheng, C. Li, W. Ni, Z. Wang, Y. Zhang, B. Wang, Free-standing N-doped carbon nanofibers/carbon nanotubes hybrid film for flexible, robust half and full lithium-ion batteries, *Chem. Eng. J.* 334 (2018) 682–690.
- [45] A. Wei, W. Li, L. Zhang, B. Ren, X. Bai, Z. Liu, Enhanced electrochemical performance of a LTO/N-doped graphene composite as an anode material for Li-ion batteries, *Solid State Ionics* 311 (2017) 98–104.
- [46] G.-H. An, E.-H. Lee, H.-J. Ahn, Well-dispersed iron nanoparticles exposed within nitrogen-doped mesoporous carbon nanofibers by hydrogen-activation for oxygen reduction reaction, *J. Alloy. Compd.* 682 (2016) 746–752.
- [47] G.-H. An, H.-G. Jo, H.-J. Ahn, Platinum nanoparticles on nitrogen-doped carbon and nickel composites surfaces: a high electrical conductivity for methanol oxidation reaction, *J. Alloy. Compd.* 763 (2018) 250–256.
- [48] D. Song, J. Park, K. Kim, L.S. Lee, J.Y. Seo, Y.-K. Oh, Y.-J. Kim, M.-H. Ryou, Y.M. Lee, K. Lee, Recycling oil-extracted microalgal biomass residues into nano/micro hierarchical Sn/C composite anode materials for lithium-ion batteries, *Electrochim. Acta* 250 (2017) 59–67.
- [49] L. Tao, Y. Huang, X. Yang, Y. Zheng, C. Liu, M. Di, Z. Zheng, Flexible anode materials for lithium-ion batteries derived from waste biomass-based carbon nanofibers: I Effect of carbonization temperature, *RSC Adv.* 8 (2018) 7102–7109.
- [50] T. Li, X. Bai, Y.-X. Qi, N. Lun, Y.-J. Bai, Fe₃O₄ nanoparticles decorated on the biochar derived from pomelo pericarp as excellent anode materials for Li-ion batteries, *Electrochim. Acta* 222 (2016) 1562–1568.
- [51] G.-H. An, Y.-G. Lee, H.-J. Ahn, Ultrafast ionic diffusion of debossed carbon nanocomposites for lithium storage, *J. Alloy. Compd.* 764 (2018) 416–423.